Article

Fault Detection and Protection Strategy for Multi-Terminal HVDC Grids Using Wavelet Analysis

Jashandeep Kaur [1], Manilka Jayasooriya [1,*], Muhammad Naveed Iqbal [1,2], Kamran Daniel [2], Noman Shabbir [2,*] and Kristjan Peterson [2]

1 Department of Engineering, Staffordshire University, Stoke on Trent ST4 2DE, UK; deepmangat194@gmail.com (J.K.); naveed.iqbal@staffs.ac.uk (M.N.I.)
2 Department of Electrical Power Engineering and Mechatronics, Tallinn University of Technology, Ehitajate tee 5, 19086 Tallinn, Estonia; kamran.daniel@taltech.ee (K.D.); kristjan.pt@mail.ee (K.P.)
* Correspondence: manilka.jayasooriya@staffs.ac.uk (M.J.); noman.shabbir@taltech.ee (N.S.)

Abstract: The growing demand for electricity, integration of renewable energy sources, and recent advances in power electronics have driven the development of HVDC systems. Multi-terminal HVDC (MTDC) grids, enabled by Voltage Source Converters (VSCs), provide increased operational flexibility, including the ability to reverse power flow and independently control both active and reactive power. However, fault propagation in DC grids occurs more rapidly, potentially leading to significant damage within milliseconds. Unlike AC systems, HVDC systems lack natural zero-crossing points, making fault isolation more complex. This paper presents the implementation of a wavelet-based protection algorithm to detect faults in a four-terminal VSC-HVDC grid, modelled in MATLAB and SIMULINK. The study considers several fault scenarios, including two internal DC pole-to-ground faults, an external DC fault in the load branch, and an external AC fault outside the protected area. The discrete wavelet transform, using Symlet decomposition, is applied to classify faults based on the wavelet entropy and sharp voltage and current signal variations. The algorithm processes the decomposition coefficients to differentiate between internal and external faults, triggering appropriate relay actions. Key factors influencing the algorithm's performance include system complexity, fault location, and threshold settings. The suggested algorithm's reliability and suitability are demonstrated by the real-time implementation. The results confirmed the precise fault detection, with fault currents aligning with the values in offline models. The internal faults exhibit more entropy than external faults. Results demonstrate the algorithm's effectiveness in detecting faults rapidly and accurately. These outcomes confirm the algorithm's suitability for a real-time environment.

Keywords: fault detection; HVDC; wavelet analysis

1. Introduction

The significant growth in electricity demand over the decades, combined with the rising need for a dependable power supply, has created a necessity for more efficient approaches to managing electricity systems. The expansion of renewable energy capacity and advancements in power electronics have steered engineers' focus towards HVDC systems, which offer greater efficiency in energy transmission compared to traditional HVAC systems [1,2]. International Energy Agency (IEA) reports expect the global energy demand to grow by 4% in 2025, which is the same as in the year 2024. According to analysis, electricity consumption will be tripled between 2023 and 2025, resulting in

electricity as one of the largest sources of energy. Renewable resources will contribute 35% towards global electricity generation, while the consumption will be from conventional and newer sectors [3,4].

The European Union's long-term strategy aims to reduce greenhouse gases by 80% by 2050. To achieve this goal, an increasing number of renewable energies have been added to the generation mix [5,6]. The Global Energy Interconnection (GEI) and India's One Sun-One World-One-Grid (OSOWOG) projects represent the essential strides towards sustainable energy solutions. GEI plans to integrate renewable energy sources worldwide through an ultrahigh voltage (UHV) transmission, reducing CO_2 emissions and facilitating efficient energy distribution. China has laid 20 UHV DC and 14 UHV AC lines spanning over 38,799 km. The strategy aims to set up domestic transmission lines mainly in Eurasia and Africa as the first stage and then expand its channel transnational and transcontinental. China is well-positioned to lead this development due to its technological capacity; however, there can be certain factors that might influence its construction, like vulnerabilities to natural disasters and cybersecurity checks. Recent economic slowdowns and geopolitical tensions over energy security pose significant challenges [6–8].

However, India's ambitious approach as a part of the international solar alliance to create a global solar energy grid to incorporate smart grid systems to share solar power ensures "the sun never sets" on energy generation. By promoting renewable energy, OSOWOG can help countries avoid carbon border taxes and align with global sustainability goals [9,10]. These projects promote promising pathways for global energy cooperation, but challenges such as infrastructure development and the transition from conventional to renewable energy sources remain significant hurdles. Thomas Elva Edison pioneered the discovery of DC current, which initially formed the basis of transmission systems. However, transmitting DC currents at low voltages over extended distances was unfeasible until the advent of mercury arc valves, which facilitated voltage conversion for longer-distance transmission [11]. Subsequent advancements in converter technologies, such as the adoption of semiconductor thyristors and IGBTs in the 1990s, have significantly improved the economic viability of HVDC transmission compared to HVAC [12].

Some of the existing projects advocate the reliability of the HVDC transmission. The North Sea Link connecting the UK and Norway has a capacity of 1400 MW and became operational in 2021. It is the longest subsea interconnector in the world, with a line distance of approximately 720 km (about 447 miles) [13,14]. Viking Link is a 1.4 GW HVDC interconnector between the UK and Denmark. It is one of the longest interconnectors in the world, spanning 767 km. It began commercial operations in December 2023 [15]. The Baihetan-Zhejiang HVDC transmission line is a high-capacity power project in China, operating at a voltage of ±800 kV. Spanning 2193 km, this transmission line has a power rating of 8 GW, making it one of the most powerful HVDC systems in the world. Completed in December 2022, the project is designed to efficiently transmit electricity from the Baihetan hydropower station in Sichuan Province to Zhejiang Province [16].

Most current HVDC projects are primarily point-to-point links intended for long-distance transmission. However, when it comes to integrating multiple generation sites into a single grid, multiterminal HVDC grids with multidirectional power flow and improved control will be the preferred choice [17]. Multiterminal HVDC grids can connect multiple nodes, such as different power plants, substations, or grids. The evolution of power electronics, particularly the development of Voltage Source Converters (VSCs), has been a game-changer for MTDC systems. VSC technology enables easier control of power flow and supports the connection of multiple terminals. Unlike the older Line Commutated Converters (LCCs), VSCs can independently control the voltage and current, making them

ideal for multiterminal configurations. VSC-based MTDC systems do not need a strong AC source, allowing for direct connection of DC links to the grid [5,18–21].

Converters play a pivotal role in HVDC systems, facilitating the conversion of AC to DC current (rectifiers) and DC to AC (inverters). The efficiency of the transmission system largely hinges on the converters employed. These converters are typically operated by controlled and non-controlled valves, also referred to as switching devices. The primary components of the converter include the converter transformer, smoothing reactor, and harmonic filters [22].

1.1. LCC Converter

LCC converters are classified as current source converters. The LCC converters utilise unidirectional DC current flow to maintain a constant output current value. Until a second zero-crossing current occurs, thyristor switches employed in the converter tend to uphold the same condition [23]. The switching frequencies of these converters align with the line frequencies and, therefore, lack black start ability. Due to the lack of frequencies in complete blackout scenarios, the black starting is unfeasible. The converter depends on the thyristor operations, hence depending on the switching voltage, which affects the functionality during a blackout. LCC-based technology is predominant in many existing projects. The single line diagram of an LCC HVDC topology is shown in Figure 1. However, there is a shift in focus towards VSC converters, as they provide independent control over reactive power [23,24].
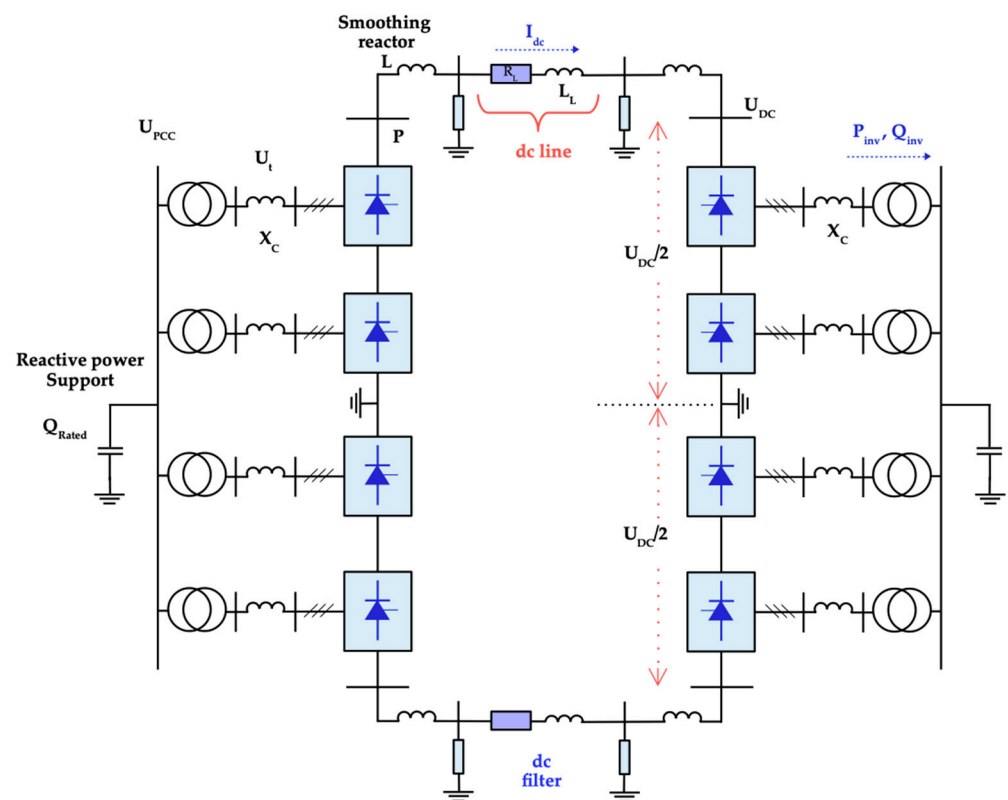

Figure 1. Single line diagram of the LCC HVDC system.

1.2. VSC Converters

VSC-based converters can be switched on and off independently of external AC voltage by utilising IGBT-controlled technology. During black starts, LCC converters have the capability to generate their own AC voltages. Pulse width modulation (PWM) adjusts the amplitude and phase angle of the converter and maintains a constant voltage.

Additionally, VSCs can operate effectively in weak AC systems. However, VSCs are more expensive and prone to higher converter losses [23–25].

New semiconductor technology includes SiC (silicon carbide), which could offer benefits for grid development. There has been remarkable development in monitoring electrical systems through the implementation of Supervisory Control and Data Acquisition (SCADA) systems [26]. The recent implementation of Controllable Line-Commuted Converter (CLCC) technology improves the performance and stability of HVDC systems. The advanced VSC-based converters using MMC technology will be most beneficial and applicable for upcoming HVDC projects [27], the converter topology for which is shown in Figure 2 below.
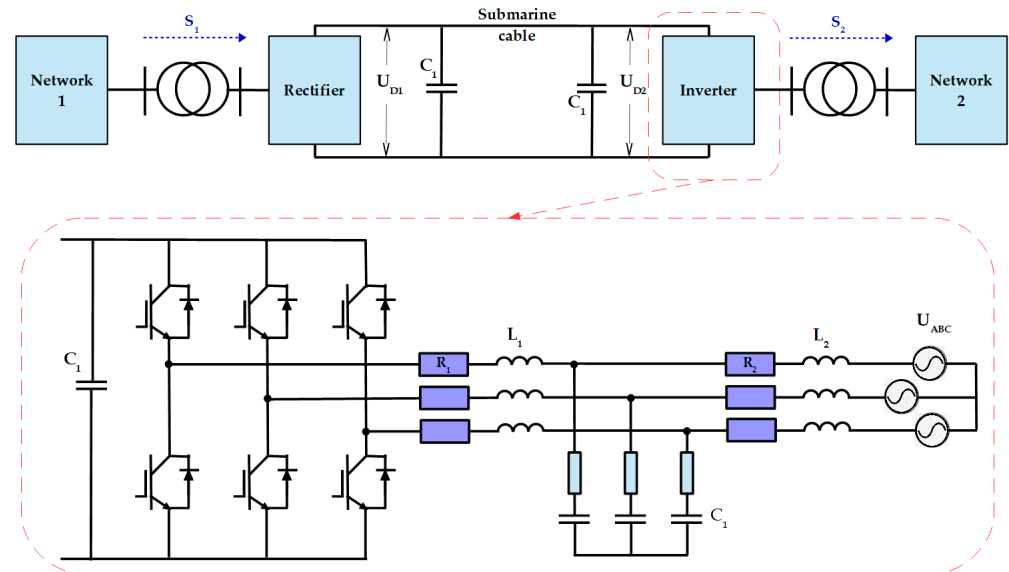

Figure 2. Structure of VSC-HVDC system.

1.3. Faults and Protection Challenges

As HVDC systems have taken over the HVAC systems, the faults occurring in these systems are distinct and can be damaging to the whole grid, which can result in blackouts. Both AC and DC faults can occur in these systems. The most common faults in DC are line-to-line and line-to-ground faults. The faults that can occur on the AC side of the rectifier and inverter can be two-line short circuit faults, single-line grounding faults, or three-phase short circuit faults. To avoid the damage, they need to be addressed. There can be faults that occur at converter stations and can be caused by malfunction of valves and controllers or commutation failure [28].

Detecting faults in DC systems is difficult as compared to faults in AC systems, as there is no natural zero crossing point in DC, due to which there is no point where current passes zero, and the faulty current can be isolated from the rest of the grid. Researchers have theoretically proposed and investigated diverse concepts for HVDC circuit breakers. These investigations have encompassed a range of HVDC circuit breaker designs, including mechanical, solid-state, and hybrid configurations. Each type offers unique characteristics and potential advantages for HVDC systems. As demand for this technology grows, it continues to mature, and HVDC breakers will be deployed in the system as needed in due course [28,29].

The propagation of faults in DC systems is more rapid compared to AC systems and can destroy a grid within milliseconds. As an alternative to HVDC breakers, advanced protection strategies have been developed to rapidly detect, locate, and isolate faults. Di/dt-based protection monitors the rate of change in current (di/dt) to detect faults at

specific locations [30]. The occurrence of faults leads to rapid changes in voltage levels, thereby triggering power semiconductor devices like thyristors and IGBTs. Snubber circuits, comprising resistors and capacitance, are employed to prevent this triggering, hence classified as dv/dt-based protection [31].

Every signal has specific characteristics in terms of frequency, size, and energy. When a fault occurs, slight changes can be observed within these characteristics. Travelling wave (TW) protection relies on the high-frequency transients produced by faults as they traverse along transmission lines. The high-frequency components within these signals can aid in pinpointing the fault location. Studies indicate the utilisation of forward and backward voltage-travelling waves generated during faults for detecting DC line faults [32,33]. Transient-based protection techniques examine transient signals, such as voltage and current waveforms, which commonly manifest immediately after the fault occurrences. Unlike the previously described methods, transient studies facilitate rapid responses to swiftly occurring faults in more versatile ways and are applicable to various system configurations [34,35]. Table 1 presents a comparison of the properties of various protection methods [36].

Table 1. Comparison of different protection methods.

Method	Reactor Usage	Communication Requirement	Protection Role	Advantages	Disadvantages
Overcurrent	Limits fault current	No	Main or backup protection	Simple; uses current measurements	Selectivity issues; limited speed
Undervoltage	Used for selectivity	No	Main or backup protection	Simple; uses voltage measurements	Cannot distinguish forward/backward faults
Travelling Waves	Defines boundaries	No	Main or part of main protection	High speed using the first incident wave	Reduced margin for long lines
dv/dt	Defines boundaries	No	Main or part of main protection	High speed using the first incident wave	Susceptible to noise; limited selectivity
di/dt	Defines boundaries	No	Main or part of main protection	High speed using the first incident wave	Susceptible to noise; limited selectivity
Current Differential	Not needed	Yes	Main or busbar protection	High selectivity and robustness	Communication delays; needs synchronised measurements
Directional Protection	Not needed	Yes	Main	High sensitivity and directionality	Communication delays; limited against high resistive faults
Wavelet Transform	Defines boundaries	No	Main or part of main protection	Very fast; detects singularities	Requires extensive simulations to set thresholds

2. Wavelet Transform

According to [31], discovering effective fault mitigation techniques is crucial. A wavelet transform is a signal processing technique that decomposes a signal into a series of wavelets with different sizes, localisations, and frequencies. The wavelet transform can be viewed as an expanded form of the Fourier transform. This technique analyses periodic and stationary signals by utilising frequency information, which results in loss

of time localisation information. However, wavelet transforms can analyse non-periodic faults by providing a time-frequency component, which ensures the presence of a fault at a certain time [37,38].

These wavelets are localised in both the time and frequency domains by decomposing the signal into shifted and scaled versions of the mother wavelet (the original signal), facilitating the analysis of signal discontinuities and abrupt changes [38]. There are two types of wavelet transforms: continuous wavelet transforms (CWT) and discrete wavelet transforms (DWT). Using wavelet transforms can be helpful in detecting any changes that can be responsible for the deviation of the results from theoretical values [39].

2.1. Continuous Wavelet Transform

(CWT) is characterised by summing all the signals multiplied by scaled and shifted versions of the wavelet function [38]. It measures the degree of similarity between the analysed signal and the mother wavelet by using a scaled mother wavelet, as defined in Equation (1). This process yields a multitude of coefficients, and the formula for this function is as follows [40]:

$$T(a,b) = \frac{1}{\sqrt{a}} \int_{-\infty}^{\infty} x(t) \Psi^* \frac{(t-b)}{a} dt. \tag{1}$$

a: scale (dilation) parameter
b: location of wavelet
Ψ: wavelet function
x: signal
$*$: complex conjugate

2.2. Discrete Wavelet Transform (DWT)

This is a more efficient and reliable method that decomposes the signal into distinct sets. Instead of generating numerous coefficients, it selects a subset of scales and positions to differentiate between low- and high-frequency components. These signals excel in denoising, feature extraction, and compression, and can be defined in Equation (2) [41].

$$\text{DWT}(y, z) = \frac{1}{\sqrt{y}} \int_{-\infty}^{+\infty} f(x) \psi \frac{(x-z)}{y} dx. \tag{2}$$

$$y = 2^j, \ z = k2^j, (k,j)\epsilon Z^2. \tag{3}$$

DWT employs the Mallat algorithm to filter the signal. This filtering process yields approximations and detailed coefficients as specified in Equations (4) and (5). The approximation coefficients represent high-scale, low-frequency components, while the detail coefficients represent low-scale, high-frequency components when subjected to low-pass and high-pass filters, respectively [12,40,41].

The coefficients are mathematically represented as follows:

$$Ca_j(e) = \sum_{le} fl_o(l_e - 2e)Ca_{j-1}(l_e), \tag{4}$$

$$Cd_j(e) = \sum_{le} fl_1(l_e - 2e)Ca_{j-1}(l_e), \tag{5}$$

where f_{lo} is the low pass filter and f_{l1} is the high pass filter.

Multi-resolution signal decomposition is an iterative procedure that divides the approximations into various frequency components, constructing a wavelet decomposition tree. A decomposition tree for a two-level wavelet is demonstrated below in Figure 3.
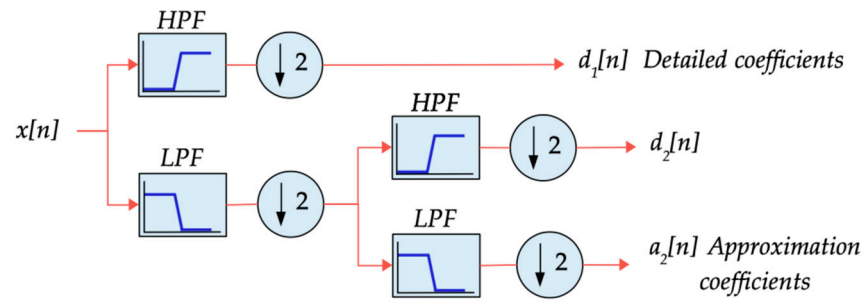
Figure 3. Two-level wavelet decomposition trees.

The mathematical representation of the decomposed signal is defined in Equation (6).

$$S(n) = \sum_{i=1}^{i} D_i(n) + A_{i(n)}. \tag{6}$$

In the time domain, Shannon entropy serves as a metric for system uncertainty. Like variations in signal frequency and amplitude, Shannon entropy is also influenced. Consequently, wavelet entropy is employed to scrutinise the information encapsulated within the frequency components of the signal [42].

The mathematical representation of wavelet entropy in terms of 'log energy' is shown in Equation (7) [43].

$$H_{logEn}(x) = -\sum_{i=0}^{N-1} (log_2(pi(x)))^2. \tag{7}$$

To calculate the energy of the detail coefficients in the j_{th} decomposition, Equations (8) and (9) are used as follows:

$$g_{aj}(e) = \sum_e \left| Ca_{j(e)} \right|^2, \tag{8}$$

$$g_{dj}(e) = \sum_e \left| Ca_{j(e)} \right|^2, \tag{9}$$

where g_{dj} is the wavelet detail coefficient energy, and g_{aj} is the approximation coefficient energy. The energy of the approximation coefficient is denoted by g_{aj} [44].

DWT leverages various wavelet families, such as Daubechies (Db), Symlets (Sym), and Coiflets (Coif), for multi-resolution signal decomposition [45]. A comparison among different wavelet families is presented in Table 2.

Table 2. Comparison of different wavelet Families [12].

Wavelet Family	Daubechies	Symlets	Coiflets	Biorthogonal	Discrete-Meyer
General form	dbN	symN	coifN	biorNr.Nd	Dmey
Members	Db1-db45	Sym2-sym31	Coif1-coif5	bior1.1-bior6.8	1
Orthogonal	Yes	Yes	Yes	No	Yes
Biorthogonal	Yes	Yes	Yes	Yes	Yes
Compact support	Yes	Yes	Yes	Yes	Yes
Filter length	2N	2N	6N	Max (2Nr,2ND)+2	102
Symmetry	Far	Near	Near	Yes	Yes
Vanishing moments numbers	N	N	2N	2Nr.	–

3. Protection Algorithm

As mentioned, discrete wavelet transforms (DWT) offer computational efficiency and can be deployed in real-time for online fault detection approaches. Hence, the wavelet trans-

form theory is applied to analyse fault characteristics within the four-terminal grid. Wavelet entropy is utilised to identify fault presence within the system using the following criteria:

If Signal Entropy $> N_f$ Signal entropy = A fault has occurred.

If Signal Entropy $< N_f$ entropy = No fault.

However, establishing a threshold for the entropy value is necessary to implement the protection strategy. The literature lacks proposed methods for identifying the threshold entropy. The values typically change due to factors such as distance and system complexity, necessitating careful consideration during threshold determination.

In this study, a systematic approach is adopted to finalise the threshold. Different threshold values were identified from various points within the subsystem, and ROC analysis was performed for these values. The results demonstrated that the threshold value of 1.555 achieves a high true positive rate (66.7%) for fault detection, eliminates false alarms (FPR = 0), and ensures system reliability compared to all other threshold values. It delivers robust overall performance with an accuracy of 73.3%, thereby validating the effectiveness of this algorithm.

The choice of mother wavelet and the number of decomposition levels impact the performance of wavelet-based fault detection [46]. During experimentation, it is crucial to establish an appropriate threshold value for no-fault entropy. This ensures that the algorithm does not miss detecting weak fault signals. For instance, if the relay point is far from the fault location, the entropy value of the signal, when it reaches the point, may be relatively low, potentially causing the fault to go undetected and leading to system damage.

Leveraging its near-symmetry and reconstruction properties, level 5 symlet decomposition is employed to extract approximate and detailed coefficients, enabling discrimination between external and internal faults. A relay threshold ('R$^{\text{th}}$') is then set to 1.5. The absolute values of the detail coefficients are compared against this relay threshold. If the coefficients exceed the relay threshold, the fault is identified as internal; otherwise, it is assumed to be an external fault.

The criteria that decide the effectiveness and reliability of the protection algorithm include its swiftness in mitigating the faults in milliseconds. The weakest faults should be ensured while the grid operates under normal conditions after fault clearances.

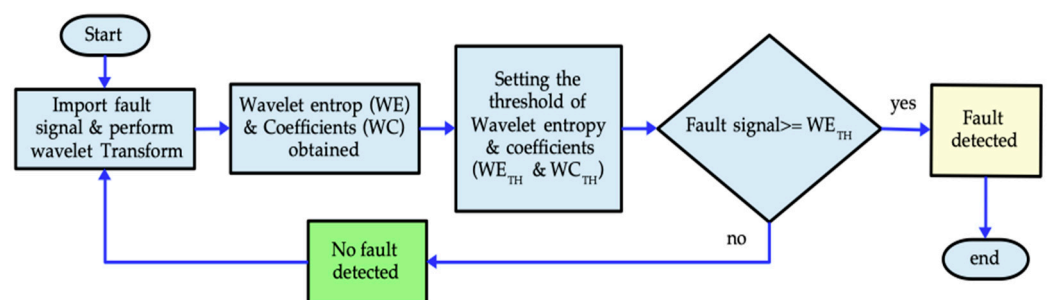The flowchart in Figure 4 illustrates the methodology employed in [12].

Figure 4. Fault detection and protection flow.

4. Simulations and Result

The four-terminal VSC HVDC grid is modelled in MATLAB/Simulink based on the multiterminal HVDC grid design proposed in [47]. The system comprises four AC terminals, each equipped with a VSC converter for bidirectional AC-to-DC conversion. Interconnecting the grid are 200 km Pi-section DC cables. A 100 kW load is linked to terminal 2 via 45 km of DC cables. DC capacitors and DC harmonic filters, as illustrated in Figure 5, and smoothing reactors are installed at the stations to mitigate distortions arising from HVDC conversion and reduce resonance. Smoothing reactors serve to minimise DC

output ripple current magnitude [48]. Additionally, 0.1-H inductors are positioned on each transmission line.
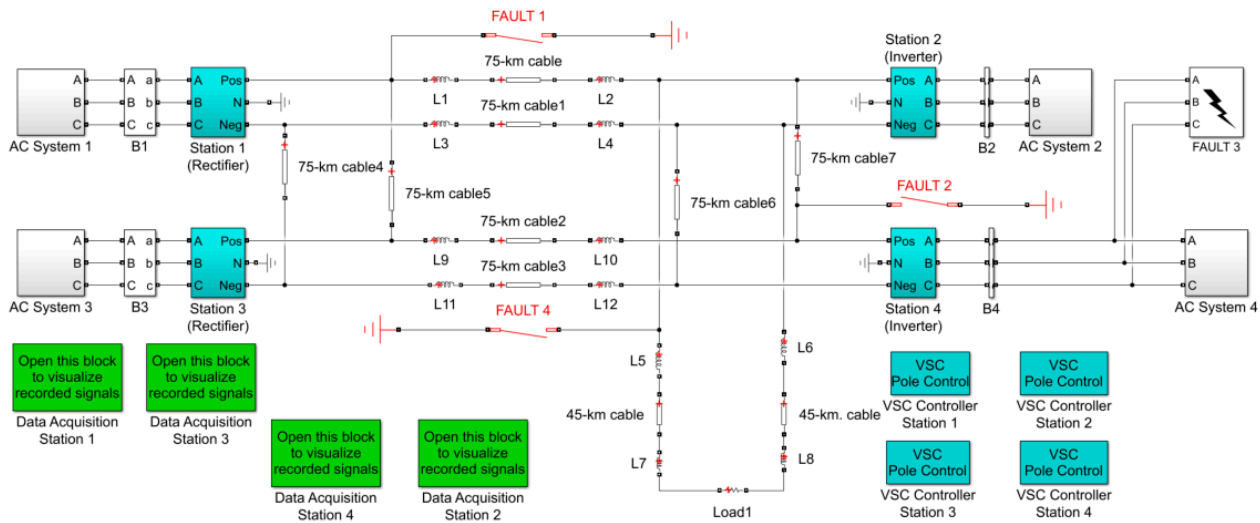

Figure 5. Simulation of four terminal VSC-HVDC systems.

Two internal DC faults near rectifier 1 (F1) and terminal 4 (F2) and an external AC fault near inverter station 4 (F3) and an external DC fault on a 45 km DC line (F4) were introduced. Fault inception time was 0.3 s, and the fault duration was 0.1 s. Both faults had 0 Ω (negligible) as fault resistance.

According to [24], the complexity of the four-terminal VSC-HVDC system presents challenges in fault detection. As the distance from the fault increases, signal characteristics undergo changes, resulting in distortions during transmission. This, in turn, significantly impacts the sensitivity of fault detection algorithms. The system's complexity also affects the entropy and wavelet coefficient values. Experiments conducted in [49] reveal that entropy values increase as the distance between the relay point and the fault point decreases.

The signal features are manipulated by the functionality of the wavelet transforms and filter length [12]. Symlets-3 filters are characterised by summing all the signals multiplied by scaled and shifted versions of the wavelet function of the original signal, which closely aligns with the properties of fault signals during signal reconstruction.

To establish parameters for distinguishing fault conditions, the system initially undergoes no-fault testing. The critical condition entropy observed at terminal 4, which is 1.2550×10^6, is established as the reference entropy for no-fault conditions. During the no-fault scenario, the system reaches a steady-state condition at 0.14 s, with the voltage approximately rising to 100 kV and the current at 0 kA on each side.

4.1. F1 and F2 Internal DC Fault

For F1, the current magnitude peaks at the fault inception time of 0.3 and continues to grow because of a low impedance path at the fault pole. For simplicity, only DC positive pole current and voltages are considered. Figures 6 and 7 show the DC fault current and voltage at the inception of internal fault F1, respectively. At the onset of the fault, the positive pole current peaks at approximately 10 kA and fluctuates between 5 kA and 2.8 kA, significantly higher than the initial current values in the absence of a fault. In contrast, the voltage quickly drops to 0 as soon as the fault occurs at 0.3 s. Coefficient values, as shown in Figure 8, remain at zero until the fault time, after which they increase relatively sharply around 0.30026 s. These non-zero coefficients signify abrupt changes in frequency when a fault occurs. Therefore, wavelet transforms detect high-frequency components during transient stages before they manifest into surges. Both current and voltage signals

react simultaneously to the fault arrival time, with the non-zero coefficients returning to zero thereafter.
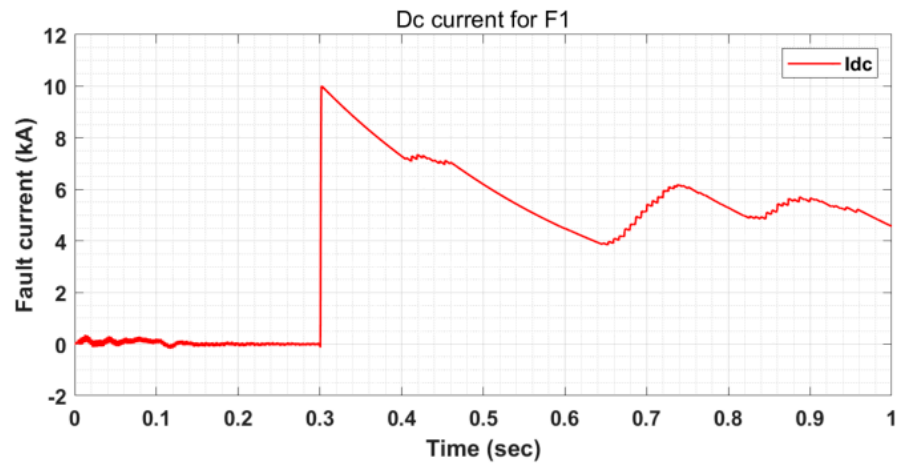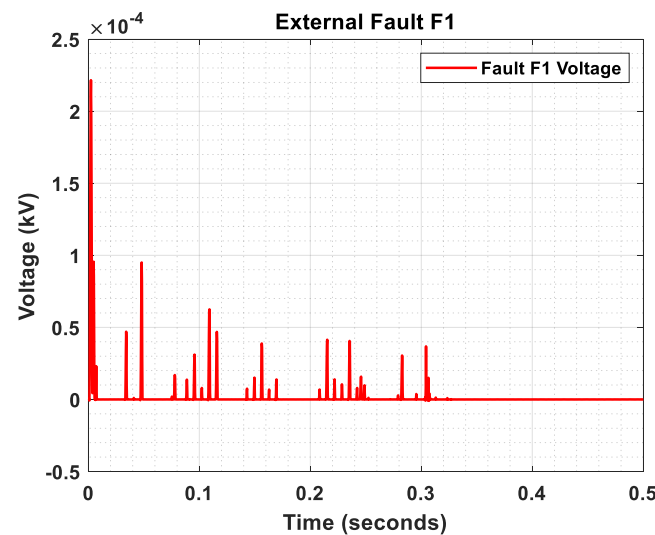

Figure 6. DC current for fault F1.

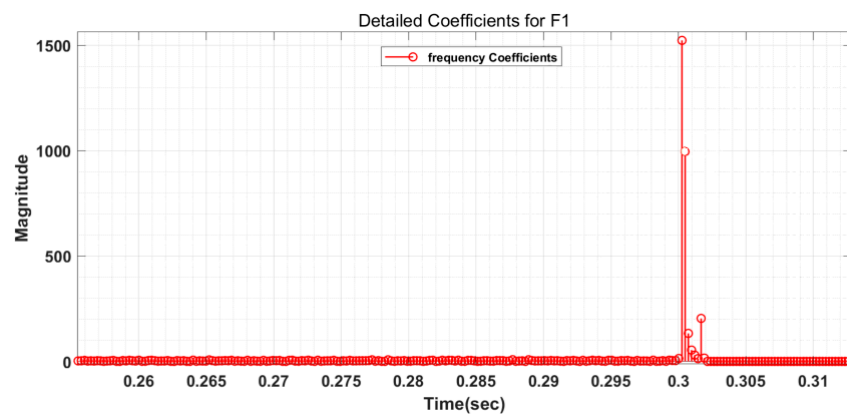**Figure 7.** Voltage for internal fault F1.

Figure 8. Detailed coefficients for F1.

Absolute coefficient values exceeding the threshold relay value of 1.5 within the time series identify the fault as an internal fault and trigger the relay accordingly.

For F2, the current signal, as shown in Figure 9, surges up to 10 kA, but in this case, it increases by a greater degree. Figure 10 demonstrates the voltage signal at the fault

inception point, which displays similar behaviour to fault F1 as it plummets towards zero. A low inductive reactance at lower frequencies in a DC line cannot prevent the DC voltage from collapsing near the faulted end, as the stored energy of the line and smoothing reactor discharges into the fault [50]. The obtained signals are influenced by harmonic distortions. At 0.3 s, which marks the fault inception time, the detail coefficients exhibit higher values, as shown in Figure 11, indicating the presence of high-frequency components in the signal. At the decomposition level focusing on these high-frequency bands, the wavelet algorithm naturally produces large coefficient magnitudes as the system tries to redistribute current instantaneously. The absolute coefficients within the time series exceed the set relay threshold, identifying the fault as an internal fault.
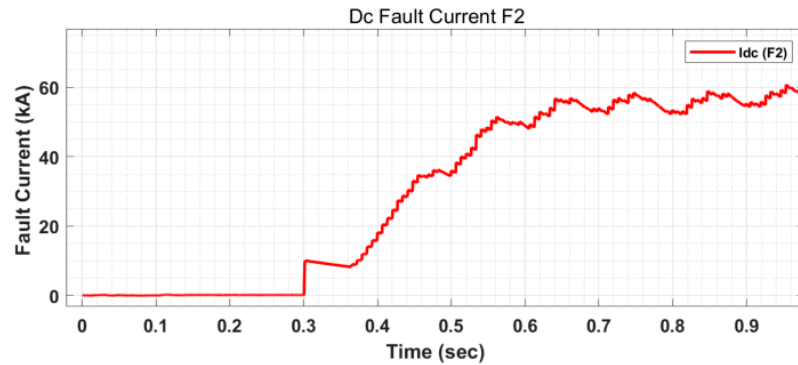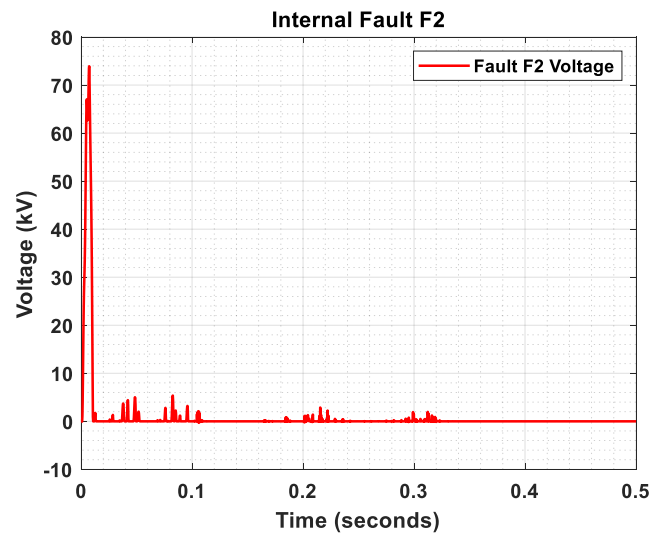

Figure 9. DC current for fault F2.

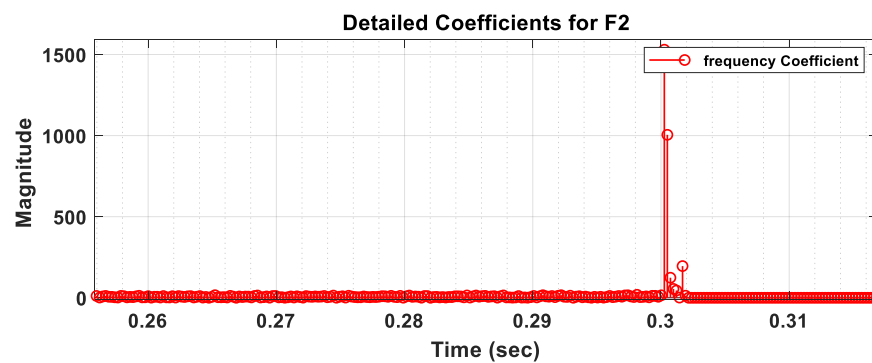**Figure 10.** Voltage for internal fault F2.

Figure 11. Detailed coefficients for fault F2.

4.2. F3 and F4 External Fault

The external faults exhibit slight differences in the output as the current reaches a higher value between 0.30026 and 0.312 s instead of 0.3 s, which influences the functionality of the protection algorithm. This delay in fault time posed a challenge in discriminating between faults, as the time ratio for fault detection changed and had to be adjusted accordingly. This limitation arises from the discrete nature of the algorithm, which does not continuously evaluate the system and may sometimes fail to detect delayed faults.

Under no-fault conditions the wavelet coefficients remain zero as observed in Figures 12 and 13. The wavelet transform theory is still validated as the system responds to the transients in the signal. The fault current value is slightly higher, as seen in Figures 14 and 15, due to the reduced distance from the relay point, causing it to nearly overlap with the internal fault value. The voltage signals for both faults, as seen in Figures 16 and 17, show a similar decrease in voltage as observed in internal DC faults. This DC link voltage drop for fault F3 is because the converter cannot sustain the DC output when the AC input is faulted. However, the algorithm successfully classifies the fault by using the detail coefficient, which in the case of an external fault is lower than that of previous internal faults.
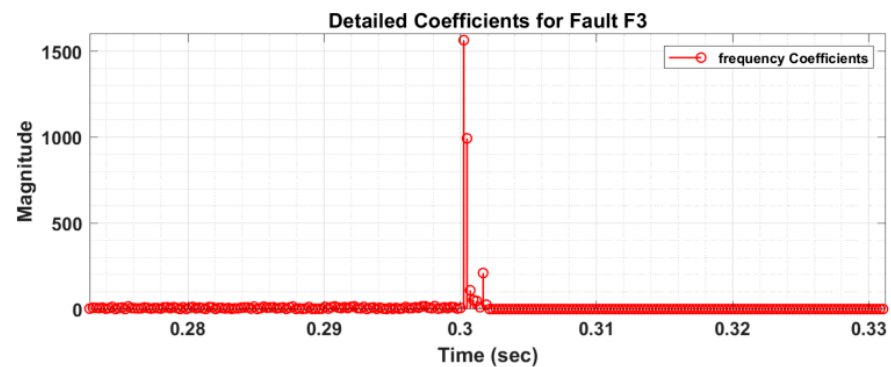

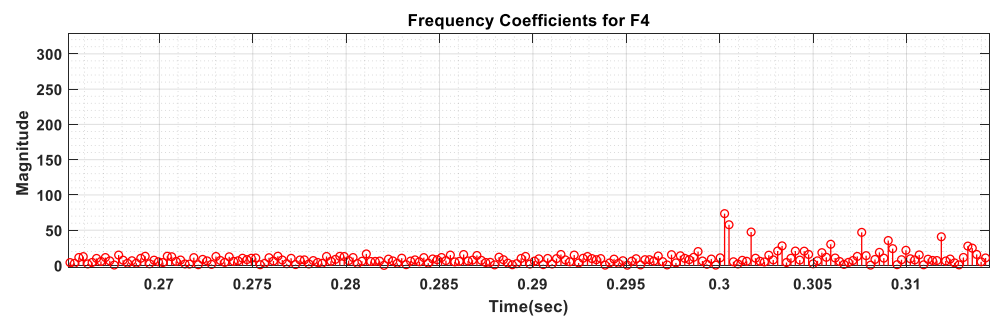**Figure 12.** Detailed coefficients for fault F3.
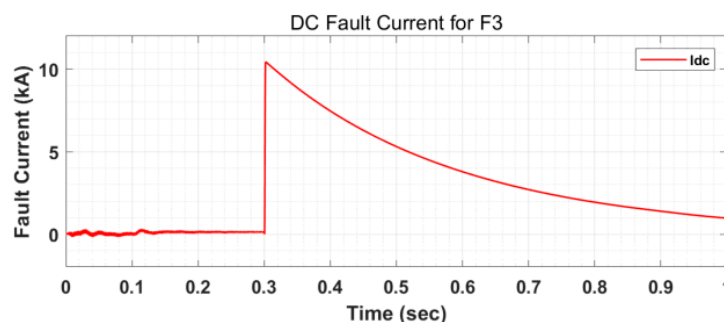

Figure 13. Detailed coefficients for fault F4.
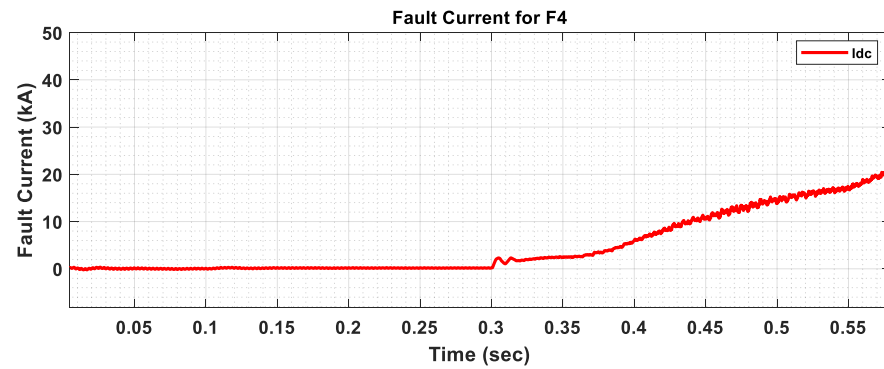

Figure 14. Current for DC fault F3.
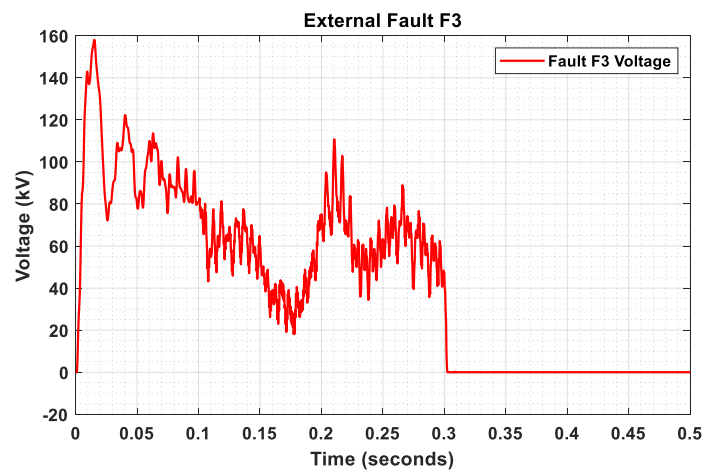
Figure 15. DC current for fault F4.

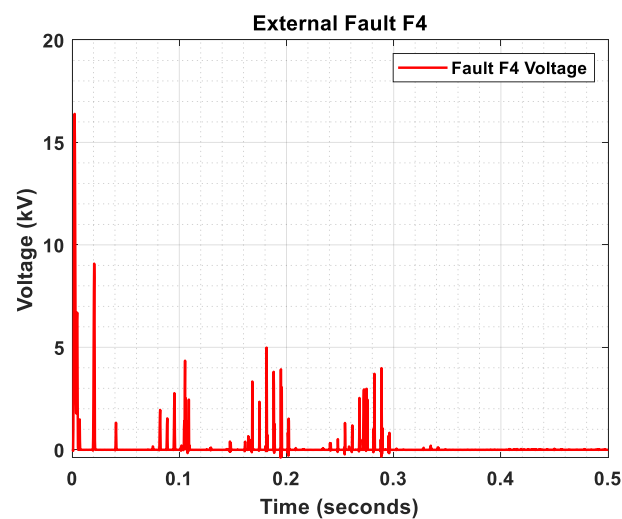**Figure 16.** Voltage for external fault F3.

Figure 17. Voltage for internal fault F4.

Figures 13 and 16 depict the general behaviour of DC fault current, and coefficients take higher values, albeit lower in comparison than all other absolute coefficient values. The absolute values are lower than the relay threshold, therefore discriminating it as an external fault.

Establishing a designated relay point and introducing a more reliable method to define fault timings within the algorithm can omit the necessity of continuously monitoring the signals. The choice of threshold values accordingly could enhance the algorithm's performance.

In this study, simulations were carried out for internal DC faults (F2) with varying resistance levels. Table 3 shows the corresponding entropy and detailed coefficient values for both the internal and external faults. As resistance increases, both entropy and detailed coefficient values decrease, which creates a critical condition for relay operation. For example, at a resistance of 0 ohms, the entropy is 2.3637×10^6, which decreases to 1.4052×10^6 at higher resistance. When approximated within a tolerance of 10%, these values converge to 1.555×10^6, which is selected as the threshold value. This threshold represents the minimum entropy for high-resistance internal faults. The results of the impact of the increase in distance on the entropy values for an internal DC fault are tabulated in Table 4.

Table 3. Entropy values for different fault scenarios.

Serial No.	Faults	Fault Entropy	Classification of Fault	Relay Operation	Error Margins ($\pm 2\sigma$)
1.	No fault	1.255×10^6	No fault	Do not trip	± 0.1336
2.	DC fault (+PG fault)	1.9402×10^6	Internal DC fault	Relay trips	± 0.4827
3.	DC fault (+PG fault)	2.3635×10^6	Internal DC fault	Relay trips	± 0.5070
4.	AC fault (3-phase ground)	1.8937×10^6	External AC fault	Do not trip	± 0.4017
5.	DC fault (external)	2.2272×10^6	External DC fault	Do not trip	± 0.2607

Table 4. Detail coefficient and entropy values for internal fault F2 with increasing resistance and distance.

Faults	Resistance (Ohm)	Distance	Entropy Values	Detail Coefficient
F2 (Internal Fault)	0	200	2.3637×10^6	1529.73
F2 (Internal Fault)	0	500	2.3252×10^6	1578.51
F2 (Internal Fault)	50	500	1.5557×10^6	1061.38
F2 (Internal Fault)	100	500	1.4605×10^6	725.441
F2 (Internal Fault)	300	500	1.3890×10^6	320.827
F2 (Internal Fault)	500	500	1.4052×10^6	204.908
F4 (External Fault)	0	200	2.2272×10^6	73.482

Typically, internal faults produce entropy values much higher than this threshold, whereas external faults generally have values below it. For DC external faults occurring at specific distances, fault discrimination is achieved using detailed coefficient values, which are notably lower for external faults compared to internal ones, aiding in their classification. Although wavelet entropy is less sensitive to high-resistance internal faults and may not effectively distinguish weaker faults, entropy values for external faults tend to exceed the threshold.

5. Real-Time Simulation Results

The real-time simulation reflects the system's behaviour under practical operating conditions, offering a more dynamic perspective. It includes hardware-induced variations, deeply analysing system response and fault characteristics.

The Simulink model, as shown in Figure 5, was designed for real-time execution using the OPAL-RT simulator. The significant components within the system include the OP-Comm block, as shown in Figure 18, which enables communication between the Simulink model and OPAL-RT. For precise real-time simulations, the ARTEMIS Guide block, as seen in Figure 19, synchronises the solver with the time step of 50 μs. SM_FINAL_MODEL is

a subsystem with four terminal grids injected for analysis. SC_FINAL_MODEL is a logic that analyses signals and establishes fault situations.
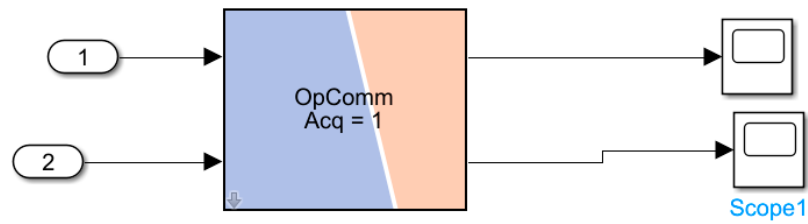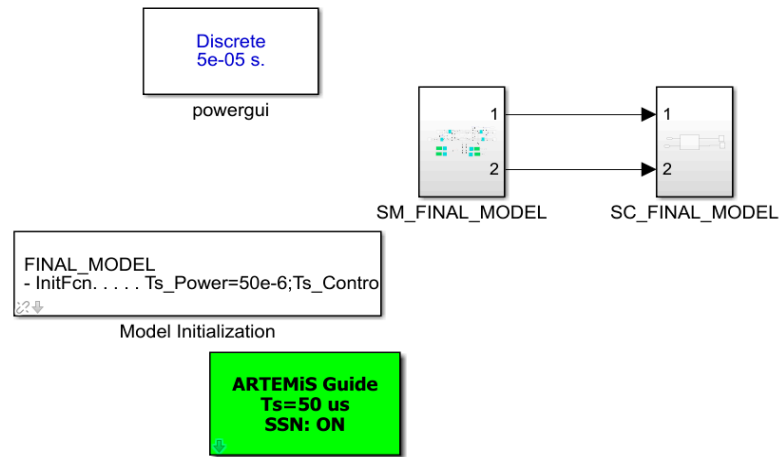

Figure 18. OpComm blocks for output.

Figure 19. Real-time model for four terminal grid.

The results obtained after real-time execution provide important insights when compared to offline simulation. The algorithm operates as expected; it differentiates between internal and external faults. The entropy for internal faults is consistently higher as compared to the external fault values. The current values reach noticeably higher peaks when a fault arises, indicating their existence and detectability. The fault current behaviour for each fault condition can be observed in Figures 20–23.
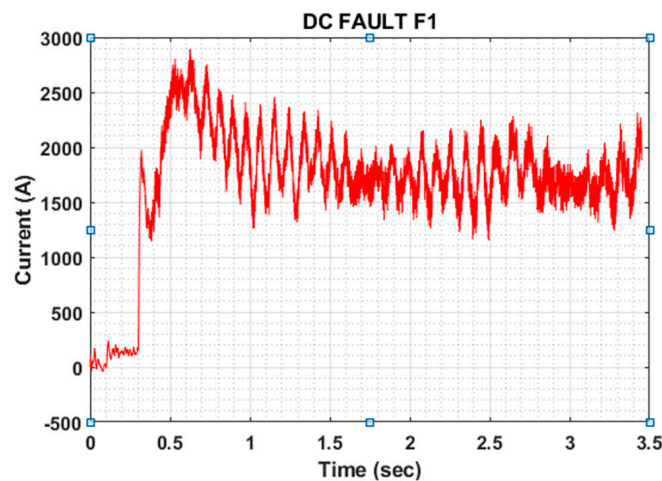

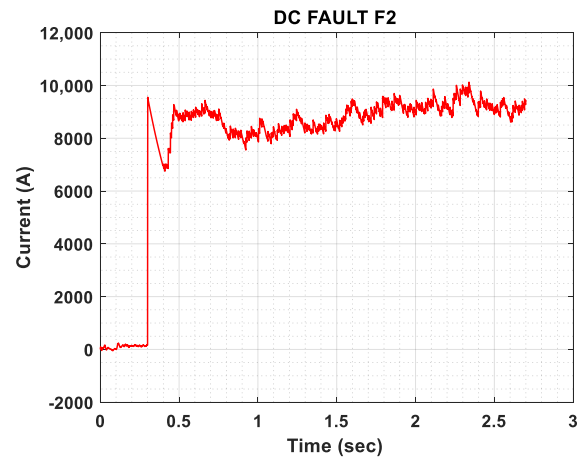**Figure 20.** Current for DC fault F1.

Figure 21. Current for DC fault F2.

Figure 22. Current for AC fault F3.
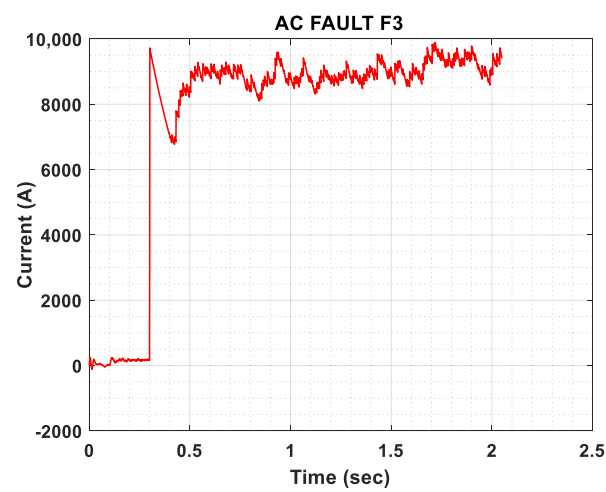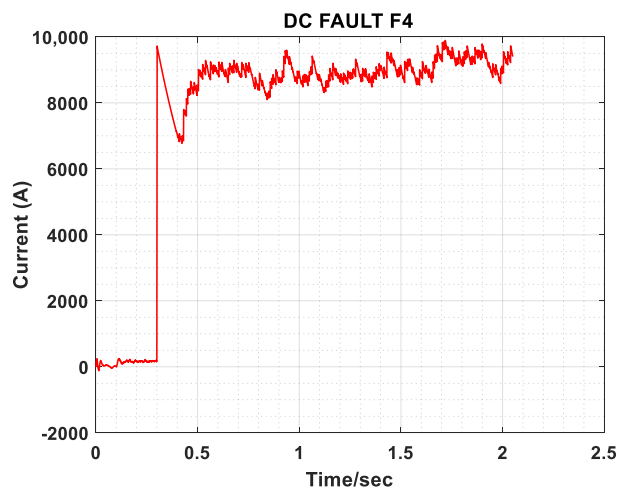

Figure 23. Current for DC fault F4.

However, when compared to offline simulation, the entropy values are lower in real-time execution. The simulation entropies for each fault case are listed in Table 5. The current values are constant in both settings, peaking at around 10 kA and higher during faults. The reason behind the lower entropies is yet unclear; however, the current behaviour

and fault detection confirm the algorithm's efficacy in offline and real-time scenarios. These outcomes confirm the algorithm's suitability for a real-time environment.

Table 5. Entropy values for real-time simulation.

No Fault Entropy	F1 Entropy	F2 Entropy	F3 Entropy	F4 Entropy
5.04×10^5	9.96×10^5	9.23×10^5	5.72	6.91×10^5

6. Conclusions

The paper attests to the effectiveness of wavelet entropy and coefficients in protecting the HVDC grids, successfully achieving its predetermined objectives. The wavelet entropy leverages fault identification, and the high-frequency coefficients obtained aid in classifying the faults in milliseconds after their occurrence. Hence, the system proves its reliability and efficiency. Nonetheless, a few factors can limit its performance. The algorithm necessitates precise methods to determine the threshold values for entropy and relay settings. Fault timings within the protection algorithm require adaptation accordingly to avert false detections, which adds complexity. While theoretically sound, the algorithm's ability to perform accurately under real-time situations highlights its dependability and appropriateness for actual HVDC systems, despite different entropy values.

Author Contributions: Conceptualization, J.K., M.J., and M.N.I.; methodology, J.K., M.J., and K.P.; software, J.K., M.J., and N.S.; validation, M.N.I., K.D., and N.S.; formal analysis, J.K., M.J., and K.D.; investigation, J.K., M.J., and N.S.; resources, J.K., M.J., and K.P.; data curation, M.N.I., K.P., and N.S.; writing—original draft preparation, J.K., M.J., and N.S.; writing—review and editing, J.K., M.J., and K.P.; visualization, J.K., M.J., and K.D.; supervision, J.K., M.J., and M.N.I.; project administration, J.K., M.J., and K.P.; funding acquisition, K.D., N.S., and M.N.I. All authors have read and agreed to the published version of the manuscript.

Data Availability Statement: Data is contained within the paper.

Conflicts of Interest: The authors declare no conflicts of interest.

References

1. Li, Z.; Zhan, R.; Li, Y.; He, Y.; Hou, J.; Zhao, X.; Zhang, X.P. Recent Developments in HVDC Transmission Systems to Support Renewable Energy Integration. *Glob. Energy Interconnect.* **2018**, *1*, 595–607. [CrossRef]
2. Atsushi, N.; Fidel, A.; Takahiro, O. *Global Innovation Report Global Rise of HVDC and Its Background*; Hitachi Review; Hitachi: Tokyo, Janpan, 2020; pp. 50–55.
3. McKinsey & Company. *Global Energy Perspective 2024*; McKinsey & Company: New York, NY, USA, 2024. Available online: https://www.mckinsey.com/industries/energy-and-materials/our-insights/global-energy-perspective (accessed on 9 December 2024).
4. IEA. *Global Electricity Demand Set to Rise Strongly This Year and Next, Reflecting Its Expanding Role in Energy Systems Around the World*; IEA: Paris, France, 2024. Available online: https://www.iea.org/news/global-electricity-demand-set-to-rise-strongly-this-year-and-next-reflecting-its-expanding-role-in-energy-systems-around-the-world (accessed on 9 December 2024).
5. Iqbal, M.N.; Kütt, L.; Rosin, A. Complexities associated with modeling of residential electricity consumption. In Proceedings of the 2018 IEEE 59th International Scientific Conference on Power and Electrical Engineering of Riga Technical University (RTUCON), Riga, Latvia, 12–14 November 2018; pp. 1–6. [CrossRef]
6. Guo, F.; van Ruijven, B.; Zakeri, B.; Krey, V.; Riahi, K. Global Energy Interconnection: A Scenario Analysis Based on the MESSAGEix-GLOBIOM Model. Available online: https://pure.iiasa.ac.at/id/eprint/17487/ (accessed on 11 November 2024).
7. Wang, M.; Kang, W.; Chen, Z.; Zhang, Y.; Liu, C.; Yang, F. Global Energy Interconnection: An Innovative Solution for Implementing the Paris Agreement—The Significance and Pathway of Integrating GEI into Global Climate Governance. *Glob. Energy Interconnect.* **2018**, *1*, 467–476. [CrossRef]
8. Jain, A.K. Sustainable Energy: One Sun-One World-One Grid. In *Climate Resilient, Green and Low Carbon Built Environment*; Springer: Berlin/Heidelberg, Germany, 2023; pp. 91–123, ISBN 978-981-99-0215-6.

9. Kadam, S.; Dhole, K.; Kumar, A.; Gupta, N.; Mishra, S. Impact of International Solar Alliance on World. *Int. J. Adv. Res. Sci. Commun. Technol.* **2023**, *3*, 233–260. [CrossRef]

10. Grid, N. North Sea Link|National Grid Group: Connecting the UK to Clean, Reliable Energy. Available online: https://www.nationalgrid.com/national-grid-ventures/interconnectors-connecting-cleaner-future/north-sea-link (accessed on 6 August 2024).

11. Mohammadi, F.; Rouzbehi, K.; Hajian, M.; Niayesh, K.; Gharehpetian, G.B.; Saad, H.; Hasan Ali, M.; Sood, V.K. HVDC Circuit Breakers: A Comprehensive Review. *IEEE Trans. Power Electron.* **2021**, *36*, 13726–13739. [CrossRef]

12. Omorogbe, P.A.; Griffiths, A.; Ikhide, M.; Tennakoon, S. An Investigation of the Distinct Features of Wavelet Transform Based Protection Strategy for Consideration in HVDC Grids. In Proceedings of the 2021 IEEE Southern Power Electronics Conference SPEC, Kigali, Rwanda, 6–9 December 2021; pp. 1–6. [CrossRef]

13. Zakeri, B.; Price, J.; Zeyringer, M.; Keppo, I.; Mathiesen, B.V.; Syri, S. The Direct Interconnection of the UK and Nordic Power Market—Impact on Social Welfare and Renewable Energy Integration. *Energy* **2018**, *162*, 1193–1204. [CrossRef]

14. Grid, N. Viking Link | National Grid Group: Sharing Clean Energy between the UK and Denmark. Available online: https://www.nationalgrid.com/national-grid-ventures/viking-link (accessed on 8 September 2024).

15. Oni, O.E.; Davidson, I.E.; Mbangula, K.N.I. A Review of LCC-HVDC and VSC-HVDC Technologies and Applications. In Proceedings of the EEEIC 2016—International Conference on Environment and Electrical Engineering, Florence, Italy, 7–10 June 2016; pp. 1–7. [CrossRef]

16. China's 8 GW Baihetan-Zhejiang Power Transmission Line. Available online: https://www.enerdata.net/publications/daily-energy-news/chinas-8-gw-baihetan-zhejiang-power-transmission-line-fully-operational.html (accessed on 19 August 2024).

17. Düllmann, P.; Klein, C.; Winter, P.; Köhler, H.; Steglich, M.; Teuwsen, J.; Leterme, W. Preventive DC-Side Decoupling: A System Integrity Protection Scheme to Limit the Impact of DC Faults in Offshore Multi-Terminal HVDC Systems. *IET Gener. Transm. Distrib.* **2024**, *18*, 3801–3816. [CrossRef]

18. Hassanifar, M.; Hrishikesan, V.M.; Jung, J.H.; Bazyar, S.; Beiranvand, H.; Pereira, T.; Langwasser, M.; Liserre, M. Modular Multilevel Converters Enabling Multibus DC Distribution. In Proceedings of the CPE-POWERENG 2023—17th IEEE International Conference on Compatibility, Power Electronics and Power Engineering, Tallinn, Estonia, 14–16 June 2023; pp. 1–7. [CrossRef]

19. Regnier, B.; Koreman, K. Measurement Transducers for LCC and VSC HVDC Converter Stations. In *High Voltage DC Transmission Systems: HVDC*; Andersen, B.R., Nilsson, S.L., Eds.; Springer International Publishing: Cham, Switzerland, 2023; pp. 1–29. ISBN 978-3-030-71619-6.

20. ChanKi, K.; Vijay, S.; Gil-Soo, J.; SeongJoo, L.; Seok-Jin, L. *HVDC Transmission: Power Conversions Applications in Power*; John Wiley & Sons: Hoboken, NJ, USA, 2009. [CrossRef]

21. Le Blond, S.; Bertho, R.; Coury, D.V.; Vieira, J.C.M. Design of Protection Schemes for Multi-Terminal HVDC Systems. *Renew. Sustain. Energy Rev.* **2016**, *56*, 965–974. [CrossRef]

22. Pipelzadeh, Y.; Chaudhuri, N.R.; Chaudhuri, B.; Green, T.C. System Stability Improvement through Optimal Control Allocation in Voltage Source Converter-Based High-Voltage Direct Current Links. *IET Gener. Transm. Distrib.* **2012**, *6*, 811–821. [CrossRef]

23. Bjarne, A.; Stig, N. *High Voltage DC Transmission Systems*; Springer: Berlin/Heidelberg, Germany, 2024; ISBN 978-3-031-27353-7.

24. Huang, W.; Luo, G.; Cheng, M.; He, J.; Liu, Z.; Zhao, Y. Protection Method Based on Wavelet Entropy for Mmc-Hvdc Overhead Transmission Lines. *Energies* **2021**, *14*, 678. [CrossRef]

25. Stan, A.; Costinaș, S.; Ion, G. Overview and Assessment of HVDC Current Applications and Future Trends. *Energies* **2022**, *15*, 1193. [CrossRef]

26. López, A.; Ferrero, F.; Yangüela, D.; Álvarez, C.; Postolache, O. Development of a Computer Writing System Based on EOG. *Sensors* **2017**, *17*, 1505. [CrossRef] [PubMed]

27. Hu, C.; Ma, Y.; Yu, J.; Zhao, L. Dynamic Surface Backstepping Control for Voltage Source Converter-High Voltage Direct Current Transmission Grid Side Converter Systems. *Electronics* **2020**, *9*, 333. [CrossRef]

28. Guo, T.; Zhang, T.; Lim, E.; Lopez-Benitez, M.; Ma, F.; Yu, L. A Review of Wavelet Analysis and Its Applications: Challenges and Opportunities. *IEEE Access* **2022**, *10*, 58869–58903. [CrossRef]

29. Yousaf, M.Z.; Mirsaeidi, S.; Khalid, S.; Raza, A.; Zhichu, C.; Rehman, W.U.; Badshah, F. Multisegmented Intelligent Solution for MT-HVDC Grid Protection. *Electron* **2023**, *12*, 1766. [CrossRef]

30. Eladl, A.A.; Saeed, M.A.; Sedhom, B.E.; Guerrero, J.M. IoT Technology-Based Protection Scheme for MT-HVDC Transmission Grids with Restoration Algorithm Using Support Vector Machine. *IEEE Access* **2021**, *9*, 86268–86284. [CrossRef]

31. Muniappan, M. A Comprehensive Review of DC Fault Protection Methods in HVDC Transmission Systems. *Prot. Control Mod. Power Syst.* **2021**, *6*, 1–20. [CrossRef]

32. Marvasti, F.D.; Mirzaei, A.; Savaghebi, M.; Jannesar, M.R. A Pilot Protection Scheme for HVDC Transmission Lines Based on Simultaneous Existence of Forward and Backward Voltage Travelling Waves. In Proceedings of the 2022 IEEE 13th International Symposium on Power Electronics for Distributed Generation Systems PEDG, Kiel, Germany, 26–29 June 2022; pp. 1–6. [CrossRef]

33. Saha, M.M.; Izykowski, J.; Rosolowski, E. Fault Location on Power Networks. *Power Syst.* **2010**, *48*, 1–422. [CrossRef]

34. Wadhwa, C.L. *Engineering Electromagnetics*; Anshan: Kent, UK SE-x, 386 Pages: Illustrations; 24 cm; Anshan Ltd.: Tunbridge Wells, UK, 2013; ISBN 9781848290785; 1848290780.

35. Wilches-Bernal, F.; Bidram, A.; Reno, M.J.; Hernandez-Alvidrez, J.; Barba, P.; Reimer, B.; Montoya, R.; Carr, C.; Lavrova, O. A Survey of Traveling Wave Protection Schemes in Electric Power Systems. *IEEE Access* **2021**, *9*, 72949–72969. [CrossRef]

36. Psaras, V.; Emhemed, A.; Adam, G.; Burt, G. Review and evaluation of the state of the art of DC fault detection for HVDC grids. In Proceedings of the 53rd International Universities Power Engineering, Glasgow, UK, 4–7 September 2018; pp. 1–6. [CrossRef]

37. Pahande, N.; Badar, A.; Patil, P. Wavelet Based Transmission Line Differential Protection Scheme. In Proceedings of the 2017 International Conference on Power and Embedded Drive Control (ICPEDC), Chennai, India, 16–18 March 2017; pp. 522–526.

38. Dutt, A. Audio Classification Using Wavelet Transform and Deep Learning. Available online: https://adityadutt.medium.com/audio-classification-using-wavelet-transform-and-deep-learning-f9f0978fa246 (accessed on 15 October 2024).

39. Taherzadeh, E.; Radmanesh, H.; Javadi, S.; Gharehpetian, G.B. Circuit Breakers in HVDC Systems: State-of-the-Art Review and Future Trends. *Prot. Control Mod. Power Syst.* **2023**, *8*, 1–16. [CrossRef]

40. Mathworks Continuous Wavelet Transform and Scale-Based Analysis. Available online: https://se.mathworks.com/help/wavelet/gs/continuous-wavelet-transform-and-scale-based-analysis.html (accessed on 11 November 2024).

41. Sundararajan, D. *Discrete Wavelet Transform: A Signal Processing Approach*; Wiley: Hoboken, NJ, USA, 2015; ISBN 9781119113119.

42. European Commission 2050 Long-Term Strategy. Available online: https://climate.ec.europa.eu/eu-action/climate-strategies-targets/2050-long-term-strategy_en (accessed on 11 August 2024).

43. Saraiva, P. On Shannon Entropy and Its Applications. *Kuwait J. Sci.* **2023**, *50*, 194–199. [CrossRef]

44. El Safty, S.; El-Zonkoly, A. Applying Wavelet Entropy Principle in Fault Classification. *Int. J. Electr. Power Energy Syst.* **2009**, *31*, 604–607. [CrossRef]

45. Zhou, B.; Sun, X.; Xu, Y.; Wei, W. Research on the Quantitative Assessment Method of HVDC Transmission Line Failure Risk during Wildfire Disaster. *Electronics* **2024**, *13*, 2119. [CrossRef]

46. Yeap, Y.M.; Geddada, N.; Ukil, A. Analysis and Validation of Wavelet Transform Based DC Fault Detection in HVDC System. *Appl. Soft Comput. J.* **2017**, *61*, 17–29. [CrossRef]

47. Kang, J.; Kang, D.W.; Lee, J.P.; Yoo, D.W.; Shim, J.W. Design Procedure of MMC-HVDC System: Comprehensive Consideration of Internal and External Dynamics. *IEEE Access* **2020**, *8*, 157437–157450. [CrossRef]

48. Ikhide, M.A. DC Line Protection for Multi-Terminal High Voltage DC (HVDC) Transmission Systems. 2017. Available online: http://eprints.staffs.ac.uk/4601/ (accessed on 9 September 2024).

49. Rong, X.; Shek, J.K.H.; Ewen Macpherson, D.; Mawby, P. The Effects of Filter Capacitors on Cable Ripple at Different Sections of the Wind Farm Based Multi-Terminal Dc System. *Energies* **2021**, *14*, 7000. [CrossRef]

50. Xue, S.; Lian, J.; Qi, J.; Fan, B. Pole-to-ground fault analysis and fast protection scheme for HVDC based on overhead transmission lines. *Energies* **2017**, *10*, 1059. [CrossRef]